Nanoporous iron oxide membranes: layer-by-layer deposition and electrochemical characterisation of processes within nanopores

Katy J. McKenzie,[a] Frank Marken,*[a] Michael Hyde[b] and Richard G. Compton[b]

[a] *Department of Chemistry, Loughborough University, Loughborough, Leicestershire, UK LE11 3TU. E-mail: f.marken@lboro.ac.uk*
[b] *Physical and Theoretical Chemistry Laboratory, Oxford University, Oxford, UK OX1 3QZ*

Received (in London, UK) 22nd January 2002, Accepted 12th March 2002
First published as an Advance Article on the web 16th April 2002

A versatile procedure for the formation of nanoporous metal oxide membranes is reported, based on a layer-by-layer deposition procedure ('directed assembly') of metal oxide nanoparticles with appropriate 'linker' molecules; here Fe_2O_3 particles and phytic acid. Two types of nanoporous Fe_2O_3 membranes have been prepared and characterised: (A) a nanofilm deposit composed of 4–5 nm diameter Fe_2O_3 particles linked by phytic acid and (B) a nanoporous film formed after calcination of the type A deposit at 500 °C in air. The nanofilm deposits are characterised by microscopy (SEM and AFM) and by electrochemical methods.

Mechanically stable and homogeneous nanofilm deposits with controlled thickness (*ca.* 3 nm per layer deposited) were obtained. Transport of small molecules or ions through the nanoporous structure and their electrochemical conversion are shown to be fast in the presence of a sufficiently high concentration of supporting electrolyte. During the electrochemical oxidation of ferrocyanide, $Fe(CN)_6^{4-}$, the nanoporous structure of the type A deposit is shown to act as an 'active' membrane, which changes the electrode kinetics by 'double-layer superposition' effects. For the second type of nanofilm, type B, ferrocyanide is accumulated by adsorption within the porous structure.

Introduction

Nanoporous membranes, and hybrid organic–inorganic membranes in particular,[1] are of considerable interest and potential technical importance, *e.g.* for filter and dialysis applications. Depending on the pore size and structure, chemical reactivity within the pores and host–guest effects (*e.g.* in zeolitic membranes) can be employed to control separation (*e.g.* for gases[2] or liquids[3]) and chemical processes.[4] Furthermore, nanoporous membranes based on inorganic materials are important and ubiquitous in nature, *e.g.* in the form of biominerals[5] or intermediates in corrosion processes.[6]

Nanoporous membranes coated onto electrode surfaces may serve various purposes, such as introducing selectivity to interfacial processes based on pore size[7] or on double-layer effects,[8,9] supporting catalysts,[10] protecting catalysts from fouling and degradation,[11] and acting as carriers for dyes in photovoltaic[12] and photochromic[13] devices. Recently, it has been shown that voltammetric techniques or 'membrane voltammetry'[14] can be employed directly for the characterisation of the properties of membranes. In the case of a 'passive' membrane, that is, a membrane with only geometry effects and no double-layer or adsorption effects, it was shown that pore size data are accessible *via* mathematical modelling of voltammetric data.

Nanoparticles are important precursors for membranes. The formation of inorganic membranes often proceeds *via* initial nanoparticle formation, *e.g.* in sol–gel-type processes.[15] Alternatively, nanoparticles with a well-defined size distribution may be prepared and then converted into close-packed nanocrystal assemblies.[16] The formation of aggregates or 'supracrystals' from nanoparticles has been reported for metal and semiconductor particles with suitable coatings.[17] We have recently proposed a layer-by-layer, or 'directed assembly', method for the formation of nanofilm deposits[18] based on a two-component dip-coating technique. This methodology is applied here for the formation of porous nanoparticle-based films. Iron oxide nanoparticles form stable colloidal solutions and readily adsorb onto glass substrates.[19] The fact that iron oxide nanoparticles adsorbed onto tin-doped indium oxide (ITO) electrodes can be detected by cathodic stripping voltammetry[20] makes these particles ideal for the study of layer-by-layer deposition processes.

In this report, it is demonstrated that well-defined nanoporous membranes may be formed by employing a layer-by-layer deposition procedure based on metal oxide nanoparticles. The size of the nanoparticles (and the size distribution) determines the pore size (and pore size distribution) of the resulting membrane. Adhesion between nanoparticles can be achieved *via* surface modification with a suitable 'linker' molecule. The formation of 'active' membranes by employing this versatile strategy is demonstrated for the case of Fe_2O_3 nanoparticles with phytic acid (see below) as the molecular 'linker'.

Experimental

Instrumentation

Electrochemical experiments were conducted with an Autolab PGSTAT30 system (EcoChemie, Utrecht, The Netherlands) in a conventional three-electrode glass cell. ITO working electrodes (tin-doped indium oxide on glass, Image Optics Components Ltd., Basildon, UK) were cut into 4 mm wide rectangular plates, cleaned by sonication in ethanol, rinsed with distilled water and subjected to heat treatment (Elite tube furnace, model TSH 12/65/550) at 500 °C in air for 60 min. These electrodes have typical resistances of 200 Ω (measured with a two point probe). A saturated Calomel electrode (SCE) served as the reference and a Pt gauze was used as the auxiliary electrode. All electrochemical experiments were con-

This journal is © The Royal Society of Chemistry and the Centre National de la Recherche Scientifique 2002

ducted at a temperature of 22 ± 2 °C. The simulation of voltammetric signals was performed with the Digisim 2™ (BAS Instruments Ltd., Congleton, UK) software package.

A Cambridge Stereoscan 360 instrument was used for SEM (scanning electron microscopy) imaging, and TEM (transmission electron microscopy) images were obtained on a JEOL 100CX system operating at 100 kV. AFM (atomic force microscopy) images were obtained *ex situ* in ambient atmosphere using a Topometrix 2010 Discoverer system with a 75 μm stage (Thermo Microscopes, Bicester, UK) in *z*-topography contact mode and typically with a 4 Hz scan rate.

Chemical reagents

Chemicals such as $FeCl_3 \cdot 6H_2O$, KCl, acetic acid, KOH (Fisher), phytic acid [*myo*-inositol hexakis(dihydrogen phosphate)], $HClO_4$ (60%) (Aldrich) $K_4Fe(CN)_4 \cdot 3H_2O$, KH_2PO_4 and K_2HPO_4 (Fisons) were obtained commercially in analytical grade quality. Filtered and demineralised water with at least 18 MΩ cm resistivity was taken from an Elgastat water purification system (Elga, High Wycombe, Bucks, UK).

Colloidal iron oxide was prepared following a literature procedure[19,21] based on dropwise addition of aqueous 20 mM $FeCl_3$ into boiling water. The resulting nanoparticles are 4–5 nm diameter in size [see Fig. 1(A)] and form a stable sol with *ca.* 2 mM content of Fe. The nanoparticles have been reported to possess the hematite (α-Fe_2O_3) structure.[21]

The procedure for the formation of nanoporous films of type A consisted of: (i) immersion of a clean ITO electrode into colloidal Fe_2O_3 solution for 1 min, then rinsing with distilled water, (ii) immersion into aqueous 40 mM phytic acid for 1 min and rinsing with distilled water (Fig. 2). By repeating this sequence, a type A nanoporous film is formed layer-by-layer. Treatment of the film deposits for 60 min at 500 °C in air in a tube furnace resulted in calcination and formation of nanoporous films of type B.

Results and discussion

Nanoparticulate Fe_2O_3 of 4–5 nm average diameter in aqueous solution readily adsorbs from a colloidal solution onto the surface of an ITO electrode. It has been shown recently[20] that the nanoparticle deposit is electroactive and that cathodic stripping occurs in aqueous buffer media at a potential which is dependent on the proton concentration. The stripping process is accompanied by the formation of Fe^{2+}(aq) and the simultaneous loss of the deposit from the electrode surface.[20]

The deposition of the Fe_2O_3 nanoparticles by adsorption is limited by the formation of a monolayer.[19] The same electrostatic forces, which prevent the precipitation of Fe_2O_3 from the colloidal solution,[22] are responsible for the monolayer adsorption limit. In order to continue the deposition process and to form a three-dimensional nanoporous film of Fe_2O_3 nanoparticles, a 'linker' molecule can be employed. In order to effectively bridge and bind to two adjacent nanoparticles the 'linker' molecule requires two or more 'binding sites'. Phosphate anions and phosphate derivatives are known to bind strongly to iron oxide surfaces.[23] Here, phytic acid (see structure) has been selected as the ideal 'linker' molecule for Fe_2O_3. Phytic acid [*myo*-inositol hexakis(dihydrogen phosphate)] is a well-known naturally occurring acid with six phosphate functional groups attached symmetrically to a cyclohexanehexol ring. It is the major phosphorous compound in plants.[24] The pK_A values for the two replaceable protons cover a range of pH values (due to intermolecular interaction of the phosphate groups) and have been reported in the range

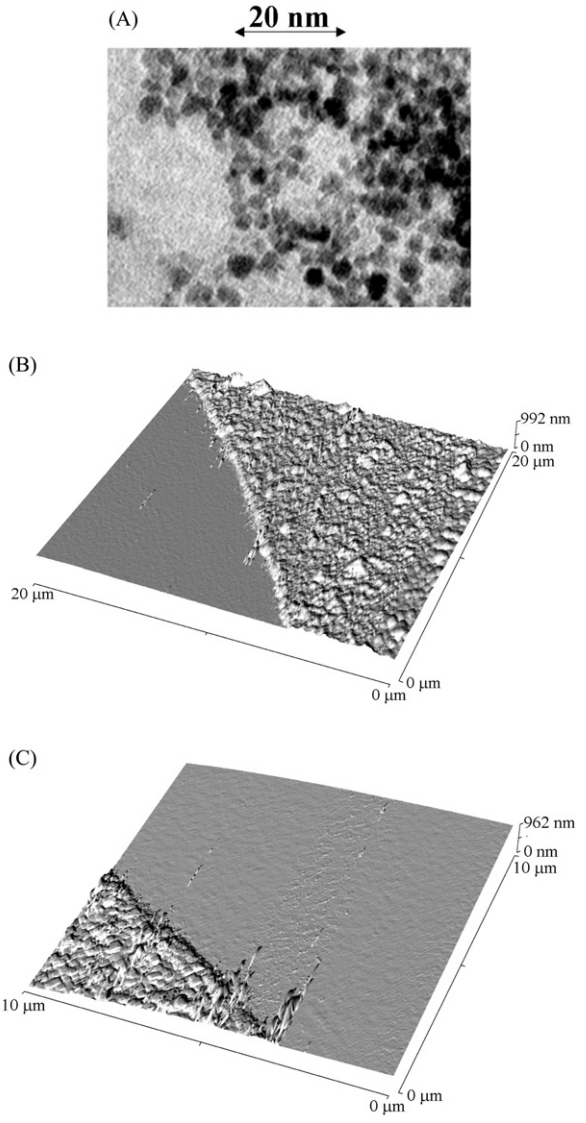

Fig. 1 (A) TEM image of Fe_2O_3 nanoparticles (deposited onto a carbon substrate) of 4–5 nm average diameter. (B) *Ex situ* AFM image of a 30 layer deposit of film type A (Fe_2O_3/phytic acid). By scratching the surface, the thickness of the deposit, *ca.* 90 nm, was evaluated. (C) *Ex situ* AFM image of a 30 layer deposit of film type B (Fe_2O_3/phytic acid after calcination at 500 °C). The thickness of the deposit is similar to that of type A films, *ca.* 90 nm on average.

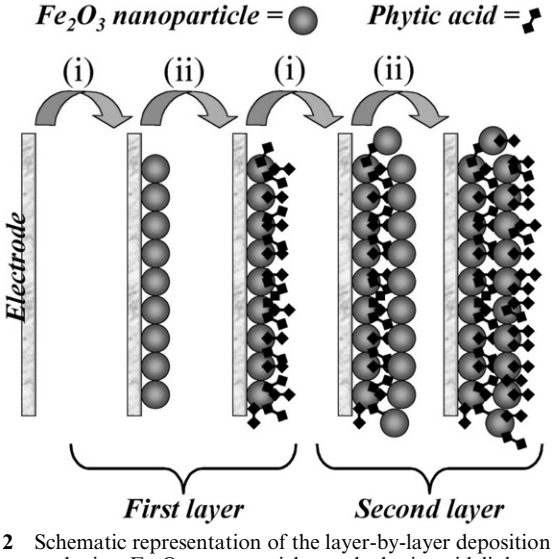

Fig. 2 Schematic representation of the layer-by-layer deposition procedure employing Fe_2O_3 nanoparticles and phytic acid linker molecules.

$pK_A^1 < 3.5$ and $pK_A^2 = 4.6$–10.[25]

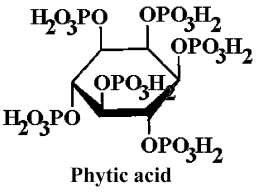

Phytic acid

Initially, experiments were conducted by immersing ITO electrode surfaces in (i) colloidal Fe_2O_3 solution (2 mM in Fe) and (ii) aqueous 40 mM phytic acid solution, with intermittent rinsing steps with water (Fig. 2). By monitoring the increase in the peak current observed for the characteristic cathodic stripping response (not shown), a first confirmation of the successful layer-by-layer deposition was obtained. However, the increase in the size of the stripping peak for multilayer deposits was not directly proportional to the number of layers applied. This was attributed to the fact that only a fraction of the Fe_2O_3 present at the electrode surface was reduced during the stripping step, which is necessarily a destructive process commencing at the point of contact between the ITO electrode and the deposit. Therefore, the charge under the stripping peak reflected only a part of the deposit and the film thickness required characterisation by independent non-electrochemical methods. The characteristic brown colour of Fe_2O_3 in multi-layer deposits is visible after application of 50 or more Fe_2O_3/phytic acid layers.

In order to quantify the formation and growth of the nanoporous Fe_2O_3 film, microscopic imaging techniques were employed. SEM images of the transition zone clean ITO electrode/Fe_2O_3 deposit (not shown) indicated the formation of a smooth and well-defined thin film deposit. AFM images [Fig. 1(B)] clearly demonstrate the formation of well-defined continuous nanofilms. By scratching the surface of the film (with a razor blade) and by imaging scratchlines for several samples with 10 to 30 deposition cycles, the thickness of the deposit was found to increase linearly with the number of layers applied. The average film growth rate can be estimated as approximately 3 nm per deposition cycle. This value is in good agreement with the anticipated growth rate based on the adsorption of layers of approximately spherical particles of 4–5 nm diameter. However, individual nanoparticles were too small to be resolved by AFM [see Fig. 1(B)].

Based on the AFM results, the nanoporous Fe_2O_3 deposit formed during layer-by-layer deposition with the phytic acid 'linker' molecule is 'homogeneous' with a well-defined average thickness. In order to characterise the properties of these films and their effect on electrochemical processes, voltammetric experiments were conducted. When immersed in aqueous 0.1 M KCl, the accessible potential window for voltammetric experiments at ITO electrodes modified with Fe_2O_3/phytic acid deposits spans from −0.2 V *vs.* SCE (reduction of Fe_2O_3) to *ca.* 1.5 V *vs.* SCE (uncharacterised anodic processes).

The oxidation of ferrocyanide anions, $Fe(CN)_6^{4-}$, (eqn. 1) occurs within this potential window and is used here as a model process for the characterisation of the properties and the transport through the porous structures.

$$Fe(CN)_6^{4-}(aq) \rightarrow Fe(CN)_6^{3-}(aq) + e^- \quad (1)$$

In Fig. 3(A) cyclic voltammograms for the oxidation of 5 mM $Fe(CN)_6^{4-}$ at modified ITO electrodes are shown. At clean ITO electrodes, a well-defined reversible oxidation with $E_{1/2} = 0.19$ V *vs.* SCE was detected. In the presence of 1 to 10 layers of Fe_2O_3/phytic acid, no significant change in the voltammetric response was seen. However, upon increasing the thickness of the nanoporous film, first a decrease in peak current and then an increase in peak-to-peak separation for the voltammetric response were found. Clearly, the nanoporous film affects the $Fe(CN)_6^{4-}$ oxidation process. However, the kinetics of the electron transfer directly at the ITO electrode surface appear to be unaffected by the initial oxide layers in direct contact with the electrode surface. The effect on voltammetric responses increases only gradually with film thickness and, therefore, appears to be associated with bulk membrane properties and/or the mass transport through the nanofilm.

Next, rotating disc electrode voltammetry experiments were conducted with 0.2 cm^2 ITO electrodes modified with Fe_2O_3/phytic acid films. In Fig. 3(B), typical steady state voltammetric responses for the oxidation of 5 mM $Fe(CN)_6^{4-}$ in aqueous 0.1 M KCl are shown. Perhaps surprisingly, the presence of the nanoporous film changes the shape of the sigmoidal voltammogram but not the mass transport-controlled limiting current (the limiting current appears to be affected only for thicker layers of Fe_2O_3, not considered here). The limiting currents for the oxidation of $Fe(CN)_6^{4-}$ show well-defined Levich behaviour and scale linearly with ferrocyanide concentration, even in the presence of the Fe_2O_3/phytic acid membrane. In Fig. 3(C) the effect of the $Fe(CN)_6^{4-}$ concentration on the electrochemical process under rotating disc voltammetry conditions is shown. The voltammetric signal scales exactly with concentration. Rescaling the individual voltammograms according to the $Fe(CN)_6^{4-}$ concentration shows that the shape of the voltammogram remains identical. This observation is consistent with that anticipated for an irreversible (slow) electron transfer step. Furthermore, this observation is a tell-tale sign for the absence of significant resistance effects,

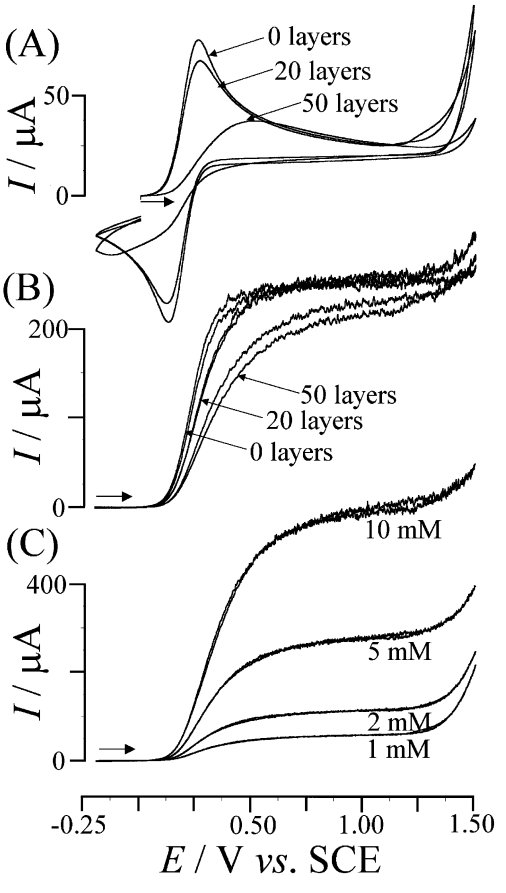

Fig. 3 (A) Cyclic voltammograms (scan rate 20 mV s^{-1}) for the oxidation of 5 mM $Fe(CN)_6^{4-}$ at a 0.2 cm^2 ITO disc electrode (clean ITO, ITO with 20 Fe_2O_3/phytic acid layers, ITO with 50 Fe_2O_3/phytic acid layers) immersed in aqueous 0.1 M KCl. (B) Cyclic voltammograms obtained under 300 rpm rotating disc conditions. (C) Cyclic voltammograms obtained at 600 rpm with concentrations of 1, 2, 5 and 10 mM $Fe(CN)_6^{4-}$.

which cause distortion of voltammetric signals as a function of concentration.

The effect of changing the concentration of the supporting electrolyte, KCl, on the voltammetric responses is very revealing. Throughout this study, a high concentration of supporting electrolyte (at least 0.1 M KCl) was employed. Fig. 4(A) demonstrates the effect of further increasing the concentration of KCl on the shape of cyclic voltammograms obtained at a 0.12 cm^2 ITO electrode modified with 50 layers of Fe_2O_3/phytic acid. The apparent rate of electron transfer increases dramatically and the shape of the cyclic voltammograms returns to that of a reversible (fast) electron transfer system.

A considerable range of possible mass transport and kinetic effects introduced by the nanoporous film during the course of electrochemical processes are known and have been reviewed.[26] Here, the effects of nanoporous films during voltammetric experiments are subdivided and discussed in terms of the following two main categories:

Case 1: the membrane is 'passive'. There are no effects introduced by the double layer of the membrane material (typical for large pores, low membrane wall capacitance and high ionic strength). With diffusion controlling the mass transport process, instead of the simple 'steady state' diffusion layer model with a diffusion layer thickness controlled by the rate of rotation, a two-layer model has to be considered. Due to the nanoscale dimension of the Fe_2O_3/phytic acid layer, typically 2 to 3 orders below that of the diffusion layer thickness observed during rotating disc electrode experiments, this effect does not dominate the process detected here. Resistance effects arising directly from the 'excluded' electrolyte volume in the nanoporous film are also possible, but they are not detected (*vide supra*) in the presence of 0.1 M KCl.

Case II: the membrane is 'active'. The double layer of the membrane causes a change in the electrochemical process (typical for small pores, high membrane capacitance and low ionic strength). Under these conditions, a multitude of complex effects are possible. However, only the case of 'double-layer superposition' will be considered here.

Both the electrode surface and the pore walls in the membrane possess double layers. Based on the pK_A of phytic acid, the membrane point of zero charge (pzc) is expected at pH < 3.5. Therefore, at a pH higher than the pzc, the resulting potential gradient within pores modifies or dominates the double layer at the electrode surface. Increasing the length of the pore induces a change in the potential distribution at the bottom of the pore. The net result on the electrochemical process occurring at the electrode surface is similar to that of a double-layer effect.[27] For a planar double layer, the apparent rate constant for the heterogeneous electron transfer, $k^0_{apparent}$, is a function of the true standard rate constant, k^0, the transfer coefficient, α, the charge of the reacting ion, z, the Faraday constant, F, the gas constant, R, the temperature, T, and the (average) double-layer potential at the outer Helmholtz plane, ϕ_2, (eqn. 2).

$$k^0_{apparent} = k^0 \exp\left(\frac{(\alpha - z)F\phi_2}{RT}\right) \quad (2)$$

The experimental results shown in Fig. 4(A) demonstrate that the Fe_2O_3/phytic acid membrane may be regarded as 'active', corresponding to case II. The membrane material imposes its own double layer onto that of the ITO electrode, and this causes electrochemical processes to change systematically. Increasing the concentration of the supporting electrolyte, KCl, allows the double-layer effect to be 'switched off'.

An attempted more quantitative analysis of the voltammograms shown in Fig. 4(A) based on numerical simulation of voltammetric responses with Digisim™ revealed that slow electron transfer kinetics based on a planar double-layer model can explain the experimental results only in part [see Fig. 4(B)]. In particular the substantial decrease in the experimental peak

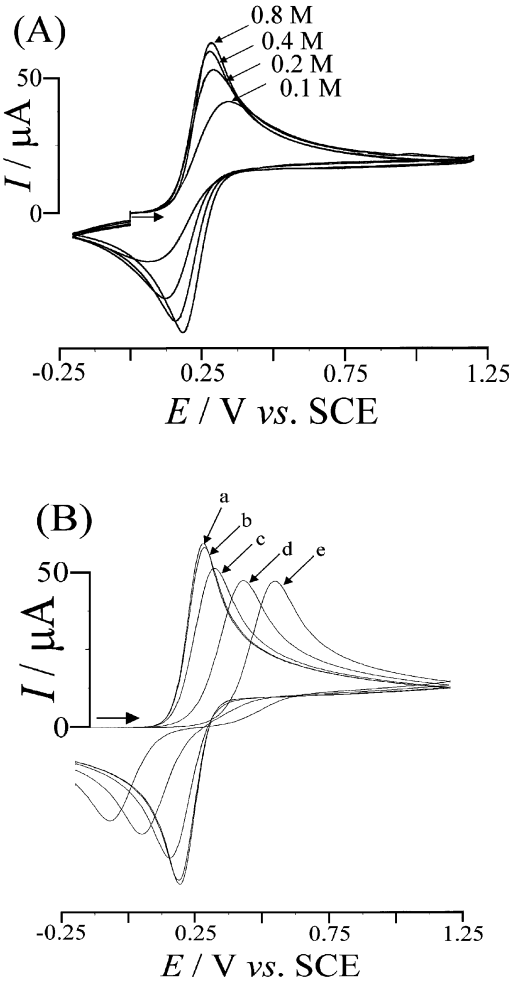

Fig. 4 (A) Cyclic voltammograms (scan rate 20 mV s^{-1}) for the oxidation of 5 mM $Fe(CN)_6^{4-}$ at a 0.12 cm^2 ITO electrode modified with film type A (50 deposition cycles in Fe_2O_3 and phytic acid). The concentration of the aqueous supporting electrolyte, KCl, was varied from 0.1 to 0.8 M. (B) Simulated (Digisim™) cyclic voltammograms (scan rate 20 mV s^{-1}), based on a slow interfacial one-electron transfer step (with $R_u = 200\ \Omega$, $\alpha = 0.5$, $k_{apparent}$: $a = 10^{-3}$, $b = 10^{-4}$, $c = 10^{-5}$, $d = 10^{-6}$, $e = 10^{-7}$ ms^{-1} and $E^0 = 0.233$ V).

current at lower KCl concentration cannot be explained. This indicates that another double-layer effect, Donnan exclusion, has to be taken into account. The potential introduced by the presence of negative charges in the membrane interior is responsible for repulsion of anions and, therefore, an energy barrier exists for negatively charged anions such as $Fe(CN)_6^{4-}$ and $Fe(CN)_6^{3-}$. As a result, the concentration of these anions in the membrane is reduced, in particular, at low supporting electrolyte concentrations. The schematic drawing in Fig. 5 illustrates this situation. The concentration of $Fe(CN)_6^{4-}$ in the membrane and in bulk solution may differ considerably. An improved numerical simulation model incorporating the concentration effect will be necessary for the quantitative interpretation of experimental voltammograms.

It is of interest to modify the Fe_2O_3/phytic acid type A nanodeposit by calcination. The result of a treatment at 500 °C in air is a purely inorganic membrane consisting of Fe_2O_3 nanoparticles, possibly coated with a layer of inorganic phosphate. An AFM study of the resulting type B film [Fig. 1(C)] demonstrates that there is virtually no change in volume before and after the calcination step. Accordingly, the dimensions of the nanopores in the structure are also preserved during calcination and no crazing occurs. The lack of calcination damage to the film is believed to be predominantly due to (i)

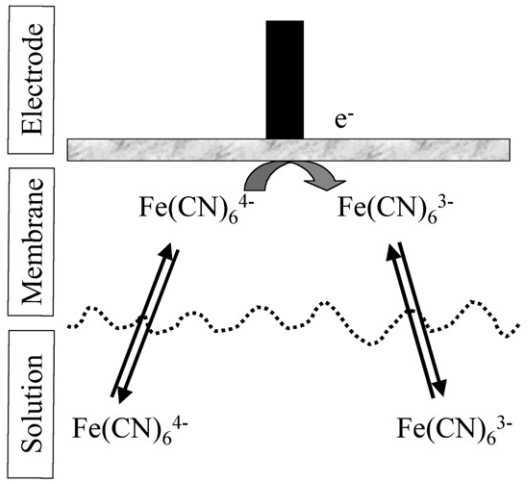

Fig. 5 Schematic drawing of the overall reaction sequences with transfer of $Fe(CN)_6^{4-}$ from solution into the membrane, reaction at the electrode surface and transfer of $Fe(CN)_6^{3-}$ back into solution.

the small volume of the carbon component of the linker molecule and (ii) the absence of long range forces (important, *e.g.* when polymeric linker molecules are employed). The stability of the film towards mechanical removal from the electrode surface is improved after calcination.

In electrochemical experiments, the porous nature of the calcined (type B) nanofilm is confirmed and the potential window accessible for electrochemical experiments is consistent with that determined for type A nanofilms. Cyclic voltammograms obtained for the oxidation of ferrocyanide in aqueous 0.1 M KCl at ITO electrodes modified with 0, 10 or 50 layers of Fe_2O_3/phytic acid (after calcination) are shown in Fig. 6. It can be seen that the properties of the nanofilm after calcination change dramatically. The size of the voltammetric response now increases with increasing thickness of the film. Clearly, accumulation of $Fe(CN)_6^{4-}$ into the porous structure occurs. Due to the replacement of phosphate anions adsorbed at the Fe_2O_3 particle surface with $Fe(CN)_6^{4-}$, a considerable amount of ferrocyanide can be bound into the structure and, therefore, the voltammetric response increases.

Results presented here from electrochemical experiments with type A and B nanofilm deposits are preliminary in nature, and a more detailed characterisation of these novel nanoporous structures and their ability to modify interfacial processes is in progress.

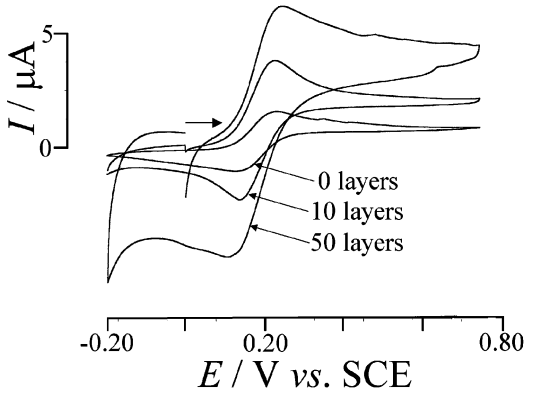

Fig. 6 Cyclic voltammograms (10 mV s^{-1}) for the oxidation of 0.1 mM $Fe(CN)_6^{4-}$ at a 0.12 cm^2 ITO electrode (clean ITO, 10 layers Fe_2O_3 type B, 50 layers Fe_2O_3 type B) immersed in aqueous 0.1 M KCl.

Conclusions

Novel nanoporous thin film deposits are formed *via* a layer-by-layer deposition method based on iron oxide nanoparticles and phytic acid 'linker' molecules. Nanofilm deposits on ITO electrodes are formed with well-defined thickness and porosity, and after calcination, the geometry of the film is preserved. The effects of the nanofilms on electrochemical processes are strongly dependent on double-layer characteristics and on the type and concentration of the supporting electrolyte.

In future, the layer-by-layer deposition technique may be employed for the formation of layered porous structures based on nanoparticles of well-defined size and/or with more than one type of nanoparticle, yielding heterostructures with extensive triple interface regions. This may lead to, for example, the development of novel electrochemical nanosensor devices and new types of membranes for interfacial reaction control.

Acknowledgements

F. M. thanks the Royal Society for a University Research Fellowship.

References

1 C. Sanchez, G. J. de, A.A. Soler-Illia, F. Ribot, T. Lalot, C. R. Mayer and V. Cabuil, *Chem. Mater.*, 2001, **13**, 3061.
2 See, for example: Y. S. Lin, *Sep. Purif. Technol.*, 2001, **25**, 39.
3 T. Tsuru, T. Sudou, S. Kawahara, T. Yoshioka and M. Asaeda, *J. Colloid Interface Sci.*, 2000, **228**, 292.
4 J. Caro, M. Noack, P. Kolsch and R. Schafer, *Microporous Mesoporous Mater.*, 2000, **38**, 3.
5 K. Simkiss and K. M. Wilbur, *Biomineralization*, Academic Press, London, 1980.
6 See, for example: M. Yamashita, H. Miyuki, Y. Matsuda, H. Nagano and T. Misawa, *Corros. Sci.*, 1994, **36**, 283.
7 See, for example: S. B. Lee and C. R. Martin, *Chem. Mater.*, 2001, **13**, 3236.
8 See, for example: C. R. Martin, M. Nishizawa, K. Jirage, M. S. Kang and S. B. Lee, *Adv. Mater.*, 2001, **13**, 1351.
9 M. Hyde, A. J. Saterlay, S. J. Wilkins, J. S. Foord, R. G. Compton and F. Marken, *J. Solid State Electrochem.*, 2002, **6**, 183.
10 See, for example: M. C. Lefebvre, Z. G. Qi and P. G. Pickup, *J. Electrochem. Soc.*, 1999, **146**, 2054.
11 See, for example: B. B. Lakshmi and C. R. Martin, *Nature*, 1997, **388**, 758.
12 See, for example: M. Grätzel, *J. Sol-Gel Sci. Technol.*, 2001, **22**, 7.
13 D. Cummins, G. Boschloo, M. Ryan, D. Corr, S. N. Rao and D. Fitzmaurice, *J. Phys. Chem. B*, 2000, **104**, 11 449.
14 B. Kralj and R. A. W. Dryfe, *Phys. Chem. Chem. Phys.*, 2001, **3**, 3156.
15 See, for example: C. J. Brinker and G. W. Scherer, *Sol-Gel Science*, Academic Press, London, 1990.
16 C. B. Murray, C. R. Kagan and M. G. Bawendi, *Annu. Rev. Mater. Sci.*, 2000, **30**, 545.
17 M. P. Pileni, in *Nanoscale Materials in Chemistry*, ed. K. J. Klabunde, Wiley, New York, 2001, p. 61.
18 R. C. Millward, C. E. Madden, I. Sutherland, R. J. Mortimer, S. Fletcher and F. Marken, *Chem. Commun.*, 2001, 1994.
19 F. Marken, D. Patel, C. E. Madden, R. C. Millward and S. Fletcher, *New J. Chem.*, 2002, **26**, 259.
20 K. J. McKenzie and F. Marken, *Pure Appl. Chem.*, 2001, **73**, 1885.
21 P. Mulvaney, R. Cooper, F. Grieser and D. Meisel, *Langmuir*, 1988, **4**, 1206.
22 P. Mulvaney, in *Nanoscale Materials in Chemistry*, ed. K. J. Klabunde, Wiley, New York, 2001, p. 121.
23 See, for example: K. Iwasaki, T. Itoh and T. Yamamura, *Mater. Trans.*, 2001, **42**, 1629.
24 *The Merck Index*, Merck & Co., Whitehouse Station, 12th edn., 1996, p. 7545.
25 H. Persson, M. Türk, M. Nyman and A. S. Sandberg, *J. Agric. Food Chem.*, 1998, **46**, 3194 and references cited therein.
26 See, for example: R. de Levie, in *Advances in Electrochemistry and Electrochemical Engineering*, ed. P. Delahay, Wiley, New York, 1967, vol. 6, p. 329.
27 A. J. Bard and L. R. Faulkner, *Electrochemical Methods*, Wiley, New York, 2nd edn., 2001, p. 571.